Acta Crystallographica Section D
Biological Crystallography
ISSN 0907-4449

Structure of a highly NADP$^+$-specific isocitrate dehydrogenase

Navdeep S. Sidhu,[a,b]* Louis T. J. Delbaere[b]‡ and George M. Sheldrick[a]

[a]Department of Structural Chemistry, University of Göttingen, Tammannstrasse 4, D-37077 Göttingen, Germany, and [b]Department of Biochemistry, University of Saskatchewan, 107 Wiggins Road, Saskatoon SK S7N 5E5, Canada

‡ Deceased 5 October 2009.

Correspondence e-mail: nsidhu@shelx.uni-ac.gwdg.de

Received 18 May 2011
Accepted 16 July 2011

PDB Reference: CglDH-Holo, 3mbc.

Isocitrate dehydrogenase catalyzes the first oxidative and decarboxylation steps in the citric acid cycle. It also lies at a crucial bifurcation point between CO_2-generating steps in the cycle and carbon-conserving steps in the glyoxylate bypass. Hence, the enzyme is a focus of regulation. The bacterial enzyme is typically dependent on the coenzyme nicotinamide adenine dinucleotide phosphate. The monomeric enzyme from *Corynebacterium glutamicum* is highly specific towards this coenzyme and the substrate isocitrate while retaining a high overall efficiency. Here, a 1.9 Å resolution crystal structure of the enzyme in complex with its coenzyme and the cofactor Mg^{2+} is reported. Coenzyme specificity is mediated by interactions with the negatively charged 2′-phosphate group, which is surrounded by the side chains of two arginines, one histidine and, *via* a water, one lysine residue, forming ion pairs and hydrogen bonds. Comparison with a previous apoenzyme structure indicates that the binding site is essentially pre-configured for coenzyme binding. In a second enzyme molecule in the asymmetric unit negatively charged aspartate and glutamate residues from a symmetry-related enzyme molecule interact with the positively charged arginines, abolishing coenzyme binding. The holoenzyme from *C. glutamicum* displays a 36° interdomain hinge-opening movement relative to the only previous holoenzyme structure of the monomeric enzyme: that from *Azotobacter vinelandii*. As a result, the active site is not blocked by the bound coenzyme as in the closed conformation of the latter, but is accessible to the substrate isocitrate. However, the substrate-binding site is disrupted in the open conformation. Hinge points could be pinpointed for the two molecules in the same crystal, which show a 13° hinge-bending movement relative to each other. One of the two pairs of hinge residues is intimately flanked on both sides by the isocitrate-binding site. This suggests that binding of a relatively small substrate (or its competitive inhibitors) in tight proximity to a hinge point could lead to large conformational changes leading to a closed, presumably catalytically active (or inactive), conformation. It is possible that the small-molecule concerted inhibitors glyoxylate and oxaloacetate similarly bind close to the hinge, leading to an inactive conformation of the enzyme.

1. Introduction

The citric acid cycle (Krebs & Johnson, 1937) is a central oxidative pathway in aerobic prokaryotes and eukaryotes. Acetate, a two-carbon (C_2) species, is fed into the cycle and fully oxidized to two molecules of CO_2, which are released into the environment. The first redox and decarboxylation steps are catalyzed by a single enzyme called isocitrate

dehydrogenase (IDH). It converts 2*R*,3*S*-isocitrate to 2-oxoglutarate and CO_2 while reducing the coenzyme nicotinamide adenine dinucleotide (phosphate) [NAD(P)$^+$] to NAD(P)H. A divalent metal ion such as Mg^{2+} or Mn^{2+} is an obligatory cofactor in both steps. The products of this reaction are utilized in biosynthesis or energy production in the respiratory chain. In bacteria and plants, IDH also lies at a point where the carbon flux can be apportioned between the citric acid cycle, in which CO_2 is generated, and a cycle variant called the glyoxylate bypass, in which both C atoms are conserved under conditions of nutritional scarcity (reviewed in Kornberg, 1966). These organisms acquire the evolutionary advantage of being able to grow on acetate, ethanol or fatty acids as their sole carbon source (Kornberg & Krebs, 1957), with the citric acid cycle and the glyoxylate pathway working in concert to balance cellular needs (Dean & Golding, 1997).

The coenzymes NAD^+ and $NADP^+$ differ from each other structurally in a simple but significant manner: the former has a hydroxyl group and the latter a phosphomonoester group at the 2′ position of the adenosine ribose, resulting in different cellular fates for the two coenzymes. IDHs tend to be specific for one or the other coenzyme (Chen & Gadal, 1990). Most bacteria contain only $NADP^+$-dependent IDH ($NADP^+$-IDH; EC 1.1.1.42); however, bacterial species in which the citric acid cycle and a terminal respiratory chain are absent, *e.g. Lactobacillus*, lack $NADP^+$-IDH (Ragland *et al.*, 1966; Chen & Gadal, 1990). Dean & Golding (1997) found that the evolution of $NADP^+$-IDHs from an NAD^+-dependent IDH (NAD^+-IDH; EC 1.1.1.41) precursor, apparently helping in niche expansion, probably occurred around the same time as eukaryotes first evolved 2–3.5 billion years ago. It has been suggested that the 2′-phosphate group enables more specific enzyme–coenzyme interactions than does the hydroxyl group and that this could explain the higher coenzyme specificities observed for $NADP^+$-dependent dehydrogenases in comparison with NAD^+-dependent dehydrogenases, with IDHs appearing to have some of the highest described $NADP^+$ specificities amongst dehydrogenases (Chen & Yang, 2000). The 80 kDa monomeric IDH recombinantly expressed from the genetic sequence of *Streptomyces lividans* TK54 prefers $NADP^+$ to NAD^+ by a factor of 60 000 (with Mg^{2+}) to 85 000 (with Mn^{2+}) (Zhang *et al.*, 2009). The monomeric IDH from *Corynebacterium glutamicum* (CgIDH; Eikmanns *et al.*, 1995) prefers $NADP^+$ by a factor of 50 000 [measured as $(k_{\rm cat,\,NADP}/K_{\rm m,\,NADP})/(k_{\rm cat,\,NAD}/K_{\rm m,\,NAD})$] with Mg^{2+} as cofactor (Chen & Yang, 2000). It is also ten times more specific for isocitrate and ten times more efficient overall $[k_{\rm cat}/(K_{\rm m,\,isocitrate}K_{\rm m,\,NADP})]$ compared with the homodimeric IDH from *Escherichia coli* (EcIDH). The latter has been reported to prefer $NADP^+$ by a factor of 7000 (Hurley *et al.*, 1996). Not all monomeric IDHs are highly specific: that from *Rhodomicrobium vannielii* has a relatively low 400-fold preference for $NADP^+$ (Leyland & Kelly, 1991).

Whereas homodimeric IDHs of approximately 40–60 kDa are present in prokaryotes and eukaryotes and include most bacterial IDHs (Chen & Gadal, 1990), 80–100 kDa monomeric IDHs similar to CgIDH have been reported exclusively in some, albeit evolutionarily diverse (Steen *et al.*, 1998), bacteria. These include *Azotobacter vinelandii* (Chung & Franzen, 1969), *Colwellia maris* (Ochiai *et al.*, 1979; Ishii *et al.*, 1987), *R. vannielii* (Leyland & Kelly, 1991), *Vibrio parahaemolyticus* (Fukunaga *et al.*, 1992) and *Desulfobacter vibrioformis* (Steen *et al.*, 1998). Furthermore, genes or putative genes encoding monomeric IDHs have been described in approximately 50 bacterial species, including pathogenic bacteria such as *Mycobacterium tuberculosis*, *M. leprae*, *Corynebacterium diphtheriae*, *Neisseria meningitidis*, *Vibrio cholerae*, *Francisella tularensis* and *Pseudomonas aeruginosa* (Yasutake *et al.*, 2002; Imabayashi *et al.*, 2006). The glyoxylate-bypass enzyme isocitrate lyase (ICL) has been shown to help *M. tuberculosis* persist in mice (McKinney *et al.*, 2000) and ICL and the two IDHs from the bacterium have been suggested as potential drug targets for tuberculosis (TB). Use in the diagnosis of TB has also been suggested for these two IDHs (Ohman & Ridell, 1996; Banerjee *et al.*, 2004), one of which is similar in sequence to monomeric IDHs, as also for a putative monomeric IDH from *M. bovis* BCG (Florio *et al.*, 2002).

Regulation of carbon flux in the citric acid cycle appears to differ significantly between the bacterial models *E. coli* and *C. glutamicum* (reviewed in Gerstmeir *et al.*, 2003). IDH and ICL compete for the substrate isocitrate. The $K_{\rm m}$ values for isocitrate of CgIDH and ICL from *C. glutamicum* are 12 and 280 μ*M*, respectively, and regulation of CgIDH activity during growth on acetate appears to be necessary (Reinscheid *et al.*, 1994; Eikmanns *et al.*, 1995). Whereas regulation of the dimeric EcIDH involves the reversible phosphorylation of a conserved Ser113 residue by IDH kinase/phosphatase (Garnak & Reeves, 1979; LaPorte & Koshland, 1982; Hurley *et al.*, 1990; Zheng & Jia, 2010), in the monomeric CgIDH concerted inhibition by glyoxylate and oxaloacetate, which decrease the enzyme activity by 50% at concentrations of 60 μ*M* each, may occur (Eikmanns *et al.*, 1995). Concerted inhibition by these metabolites of the glyoxylate and citric acid cycles has previously been reported for other dimeric and monomeric IDHs (Shiio & Ozaki, 1968; Ochiai *et al.*, 1979; Leyland & Kelly, 1991). However, the precise mechanism of regulation in monomeric IDHs remains unclear. Amongst other IDH isozymes, regulation of activity in eukaryotic hetero-oligomeric NAD^+-IDHs is allosteric, including that by adenosine monophosphate and diphosphate (Taylor *et al.*, 2008, and references therein), and self-regulation has been proposed in human cytosolic $NADP^+$-IDH (HcIDH; Xu *et al.*, 2004).

Although the structure-based sequence homology between monomeric and dimeric IDHs is only 7–8%, the tertiary structure of monomeric IDHs (Yasutake *et al.*, 2002; Imabayashi *et al.*, 2006) is similar to that of the well studied dimeric EcIDH (Hurley *et al.*, 1989) and the closely related isopropylmalate dehydrogenase (IPMDH; Imada *et al.*, 1991). Residues binding the substrate isocitrate–Mn^{2+} complex are also highly conserved between the two IDHs (Yasutake *et al.*, 2002). Coenzyme binding in homodimeric IDHs from five organisms has been described in crystal structures of EcIDH (Hurley *et al.*, 1991; Stoddard *et al.*, 1993, 1998; Bolduc *et al.*,

1995; Mesecar *et al.*, 1997), wild-type human cytosolic $NADP^+$-IDH (HcIDH; Xu *et al.*, 2004) and its cancer-associated R132H mutant (Dang *et al.*, 2009; Yang *et al.*, 2010), $NADP^+$-IDH from *Aeropyrum pernix* (ApIDH; Karlstrom *et al.*, 2005), NAD^+-IDH from *Acidithiobacillus thiooxidans* (Imada *et al.*, 2008) and *Saccharomyces cerevisiae* mitochondrial $NADP^+$-IDH (ScIDH; Peng *et al.*, 2008). A 3.2 Å resolution structure of the monomeric AvIDH in a binary complex with the coenzyme $NADP^+$ (AvIDH-Holo; Yasutake *et al.*, 2003; PDB entry 1j1w) has been described. The enzyme was in a closed, apparently inactive, conformation that lacked sufficient space for isocitrate in the active site, which was hidden under the bound $NADP^+$. An open conformation of a monomeric IDH was described in the 1.75 Å resolution structure of CgIDH in a binary complex with Mg^{2+} (CgIDH-Apo1; Imabayashi *et al.*, 2006; PDB entry 2b0t). Here, we report the 1.9 Å resolution crystal structure of the CgIDH–$NADP^+$–Mg^{2+} ternary complex (CgIDH-Holo) in an open conformation, with a second enzyme molecule in the asymmetric unit present in a binary complex with Mg^{2+} in the $NADP^+$-free form (CgIDH-Apo2).

2. Methods

2.1. Protein crystallization

The *icd* gene that encodes CgIDH has been isolated and cloned (Eikmanns *et al.*, 1995). Wild-type CgIDH was overexpressed and purified as described previously (Audette *et al.*, 1999; Bai *et al.*, 1999; Imabayashi *et al.*, 2006). Purified protein was stored at 193 K as a 10 mg ml^{-1} solution in 25 m*M* 2-morpholinoethanesulfonic acid buffer pH 6.2 with 2.5 m*M* $MnSO_4$, 2.5 m*M* dithiothreitol and 10% glycerol and was diluted with an equal volume of distilled autoclaved water immediately before use. Crystallization trials were performed using the hanging-drop vapour-diffusion method at 295 K. The reservoir solution consisted of 25%(*w*/*v*) polyethylene glycol 2000 monomethyl ether (PEG 2000 MME), 0.2 *M* tris-(hydroxymethyl)aminomethane–HCl (Tris buffer) pH 7.3 and 0.2 *M* $MgCl_2$. A separate solution with the composition of the reservoir solution with an additional 10 m*M* β-$NADP^+$ (Sigma–Aldrich) was used to form the drops by mixing 1 µl of this solution with an equal volume of the 5 mg ml^{-1} CgIDH solution. The drops were equilibrated over 0.5 ml reservoir solution. Crystals of various habits took between 3 d and two months to form. Cryoprotection was performed in two steps by adding to the drop 2 µl reservoir solution with 20 and 30% glycerol. Cracking of the crystal into a large and two smaller parts was observed during cryoprotection. The largest part was harvested within 1 min and flash-frozen in liquid N_2. The time from crystallization setup to freezing was five weeks.

2.2. Data collection

Single-crystal X-ray diffraction data were collected on the 08ID-1 beamline at the Canadian Light Source using monochromatic radiation of wavelength 0.9793 Å on a MAR Mosaic 225 mm CCD detector; a total of 633 images were collected using an oscillation range of 0.30° per image. The crystal diffracted to 1.8 Å resolution, but the data were processed to 1.9 Å owing to low completeness in the 1.9–1.8 Å resolution shell. Data reduction was performed using *XDS* (Kabsch, 2010) and scaling was performed using *XSCALE*; 5% of the data (5992 reflections) were set aside randomly as the test set for cross-validation. The crystal space group was determined to be *C*2, with two molecules in the asymmetric unit. Data-collection and processing statistics are listed in Table 1.

Table 1
Data-collection and refinement statistics.

Values in parentheses are for the outermost resolution shell. The number of atoms is the occupancy sum; *B* factors are occupancy-weighted means.

Space group	*C*2
Unit-cell parameters	
a (Å)	128.8
b (Å)	52.7
c (Å)	236.4
β (°)	103.4
Data collection	
Wavelength (Å)	0.9793
Resolution range (Å)	19.7–1.9 (1.95–1.90)
No. of reflections measured	438308
No. of unique reflections	119827
Multiplicity	3.66 (3.25)
R_{meas}	0.103 (0.364)
Completeness (%)	97.8 (85.4)
Mean $I/\sigma(I)$	9.94 (3.54)
Refinement	
Resolution limit (Å)	19.7–1.90
R_{free} (5992 reflections)	0.229
R_{work}	0.189
Total No. of reflections (working set)	113834
Solvent content (%)	49.5
No. of molecules in the asymmetric unit	2
No. of non-H atoms refined	12027
No. of water molecules refined	794
Mean *B* factors (Å^2)	
Protein atoms	38.2
Backbone atoms	37.0
Side-chain atoms	39.5
$NADP^+$	43.6
Water atoms	36.3
Protein atoms, *A* chain	26.3
Protein atoms, *B* chain	50.2
R.m.s.d.s from ideal geometry	
Bond lengths (Å)	0.012
Bond angles (°)	1.3
Ramachandran statistics	
Favoured region (%)	97.9
Allowed region (%)	2.1
Outlier region (%)	0.0

2.3. Structure solution and refinement

The structure was solved by molecular replacement (MR) with the program *Phaser* (McCoy *et al.*, 2007) as part of the *CCP*4 suite of programs (Winn *et al.*, 2011), using the previously solved CgIDH apoenzyme structure (Imabayashi *et al.*, 2006; PDB entry 2b0t) as a search model. No solution could be found if the MR search was performed using the coordinates of CgIDH-Apo1 as a whole. However, splitting CgIDH-Apo1 along its approximate interdomain boundary into two parts, one consisting of residues 2–138 and 558–736 and the other of residues 139–557, led to success. No major

clashes were observed for the best solution. Model rebuilding was performed using the program *Coot* (Emsley *et al.*, 2010). Maximum-likelihood refinement of model coordinates against the working-set data was carried out as implemented in the program *REFMAC*5.5 (Murshudov *et al.*, 2011) as part of the *CCP*4 suite. Twofold noncrystallographic symmetry (NCS) averaging with tight restraints in *REFMAC* was used initially. The NCS restraints were subsequently relaxed and finally excluded. The initial R_{work} and R_{free} were 32.0% and 31.5%, respectively. Manual modelling was carried out between a total of 28 macrocycles of refinement. Values of R_{free} (Brünger, 1992) and free log likelihood were used as a guide in determining the optimal refinement and model-building strategy throughout. Protein φ and ψ angles were not restrained during refinement. The results of model validation using the *MolProbity* server (Davis *et al.*, 2007; Chen *et al.*, 2010) were used as an additional guide in model building. Water molecules were added automatically using the program *Coot* and then inspected manually; some water molecules were added manually. Waters were, as a general rule, removed from the model if the nearest atom was closer than 2.3 Å (except for Mg^{2+} ligands and correlated half occupancies) or further than 3.5 Å, or if there was poor electron density. In the final macrocycles, H atoms were added in riding positions and TLS anisotropic displacement parameters (Schomaker & Trueblood, 1968) were refined, both as implemented in *REFMAC*, with individual *B* factors first set to a constant value of 20 $Å^2$ and followed, upon convergence, by refinement of atomic coordinates and individual *B* factors (Winn *et al.*, 2001). Three TLS groups per CgIDH molecule were defined, consisting of residues 2–138, 139–557 and 558–736. The *TLSMD* server (Painter & Merritt, 2006) was used to verify the appropriate number of TLS groups and to validate the TLS parameters of the final model. Both TLS refinement and the inclusion of H atoms in riding positions led to significant decreases in R_{free}. Analysis of TLS parameters was performed using the program *TLSANL* (Howlin *et al.*, 1993) as part of the *CCP*4 suite. $NADP^+$ coordinates were taken from the *REFMAC* monomer library within *Coot* and its final occupancy was estimated at approximately 0.9 by trial and error followed by inspection of the difference electron density and comparison of refined *B* factors with those of neighbouring protein atoms. Some alternative side-chain rotamers were modelled.

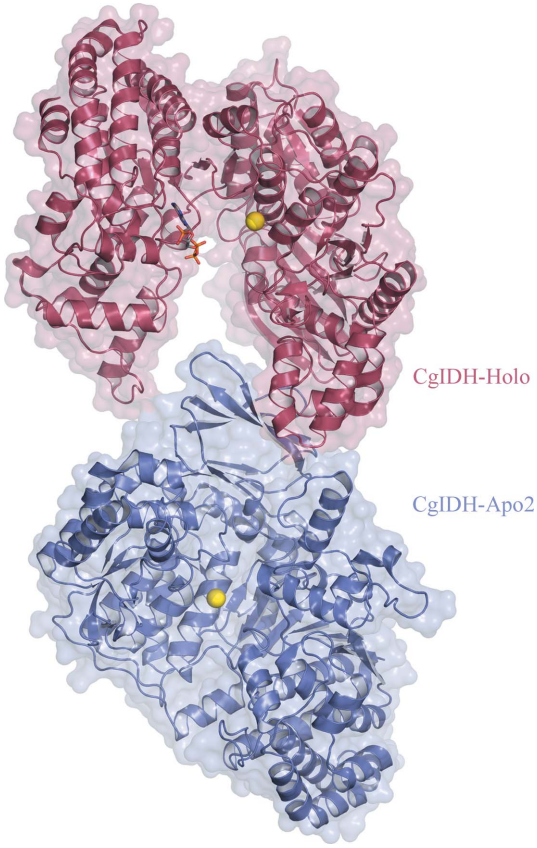

Figure 1
The asymmetric unit. The asymmetric unit contains a holoenzyme molecule (CgIDH-Holo, maroon) with the coenzyme $NADP^+$ (stick model in standard colours) and cofactor Mg^{2+} (yellow ball) bound and an apoenzyme molecule (CgIDH-Apo2, blue) with Mg^{2+} bound. Waters are omitted for clarity.

2.4. Structure analysis

Protein domains and hinge points in the present structure were determined using the program *DYNDOM* (Hayward & Berendsen, 1998) as part of the *CCP*4 suite. Structures were superimposed and r.m.s.d.s were calculated using the *CCP*4 suite program *LSQKAB* (Kabsch, 1976), which was also used to calculate changes in interdomain angles between monomeric IDH molecules based on the rotation required to superimpose domains II after the superposition of domains I. Hydrogen bonding was evaluated by adding H atoms to the protein using the *MolProbity* server. Distances and angles were calculated using *Coot*, except for the angles between aromatic ring planes, which were calculated using an in-house program (N. S. Sidhu, unpublished work). Figures were generated using the program *PyMOL* v.1.2 (DeLano, 2002). Secondary-structure assignment was performed according to the *DSSP* algorithm (Kabsch & Sander, 1983) as implemented on the *WHAT IF* server (Vriend, 1990), which was also used to determine crystal-packing contacts. Sequences of monomeric IDHs or putative monomeric IDHs (see Supplementary Material[1]) from 21 species, referred to as 'representative sequences' in the text below, were located using the National Center for Biotechnology Information (NCBI) website. Sequence alignments were performed using the program *Indonesia* (Madsen *et al.*, 2002).

3. Results

3.1. Structure solution

The 1.9 Å resolution crystal structure of the monomeric isocitrate dehydrogenase from *C. glutamicum* (CgIDH; an 80 kDa protein with 738 amino acids) cocrystallized with $NADP^+$ and Mg^{2+} was solved by molecular replacement using

[1] Supplementary material has been deposited in the IUCr electronic archive (Reference: BE5177). Services for accessing this material are described at the back of the journal.

the previously solved CgIDH apoenzyme structure (CgIDH-Apo1; Imabayashi *et al.*, 2006; PDB entry 2b0t) as the search model. The final model in the asymmetric unit (Fig. 1) consists of two CgIDH molecules (*A* and *B* chains) with 735 (2–736) amino-acid residues each, one $NADP^+$ molecule bound to chain *A* (the holoenzyme; CgIDH-Holo) while chain *B* is $NADP^+$-free (the apoenzyme; CgIDH-Apo2), one Mg^{2+} ion per CgIDH molecule and 796 O atoms (number unadjusted for occupancy) of water molecules (614 in chain *A* and 182 in chain *B*). The coordinates and structure-factor data have been deposited in the Protein Data Bank (PDB; accession code 3mbc).

3.2. Model quality

Electron density for CgIDH-Holo was in general significantly clearer than for CgIDH-Apo2. In CgIDH-Holo 50 residues are involved in crystal-packing contacts, compared with 30 in CgIDH-Apo2 as determined using the *WHAT IF* server (Vriend, 1990). This could be partly responsible for the different quality of electron density seen for the two molecules and for the lower number of water molecules modelled in the latter. The surface residue Asp306 lies in poor density in both CgIDH molecules, markedly so in CgIDH-Apo2, but was included in the model. Parts of several surface side chains in CgIDH-Apo2 had no clear density; these atoms were not included in the model. Electron density for the adenosine 2′-phosphomonoester part of $NADP^+$ was clear and exhibited sharp features, suggesting a higher degree of order, except in the neighbourhood of the C5 atom of the ribose, which lies in poorer density than the adjoining parts; density for the 5′-diphosphate was clear but less sharp, suggesting some disorder in this region. This is reflected in the higher *B* factors for the diphosphate backbone compared with the adenosine 2′-phosphate part. No clear density was observed for the nicotinamide nucleoside moiety of $NADP^+$, which is solvent-exposed in the open conformation of the enzyme. Attempts to model this moiety failed and it was not included in the model. Difference density in this region was assumed to correspond to waters, although we are unable to exclude the possibility that some of this density corresponds to unmodelled disorder in the nicotinamide nucleoside moiety. Apart from the two Mg^{2+} ions modelled in their binding sites, no attempt was made to model inorganic ions. Data-processing, refinement and validation statistics are listed in Table 1.

Protein φ and ψ angles were not restrained in refinement and thus could be used as an indicator of model quality. The Ramachandran plot shows 97.9% of amino-acid residues in the favoured region, 2.1% in the allowed region and none in the outlier region (Ramakrishnan & Ramachandran, 1965; Lovell *et al.*, 2002). The final R_{free} value was 22.9% and R_{work} was 18.9%. The *MolProbity* score was 1.47 (96th percentile; Davis *et al.*, 2007; Chen *et al.*, 2010).

3.3. Overall structure

The overall structure of both CgIDH molecules in the asymmetric unit is similar to previously determined monomeric IDH structures, especially CgIDH-Apo1, but also AvIDH-Iso (Yasutake *et al.*, 2002) and AvIDH-Holo (Yasutake *et al.*, 2003). The CgIDH apoenzyme structure, CgIDH-Apo1, has been described previously (Imabayashi *et al.*, 2006). The CgIDH holoenzyme structure will be discussed below and compared with the apoenzyme and other structures as appropriate.

CgIDH-Holo adopts an open conformation and consists of 26 α-helices (α1–α26) and 24 β-strands (β1–β24) distributed over two domains (Fig. 2): a smaller domain I (313 residues, numbered 1–138 and 564–738 in the sequence) and a larger domain II (425 residues, 139–563). Domain I thus contains both the N- and C-termini. The domain boundary on the N-terminal side (residues 138–139) falls in the α6–β4 loop and that on the C-terminal side (563–564) within strand β23. A ten-strand interdomain β-sheet (strands β1–β4, β15 and β20–β24) runs through the two domains. Domain I contains 13 α-helices (α1–α6 and α20–α26), four complete β-strands (β1–β3 and β24) and part of strand β23. All of the β-strands in this domain are part of the interdomain β-sheet. Domain II contains 13 α-helices (α7–α19), 19 complete β-strands (β4–β22) and part of strand β23. Domain II also contains a pseudo-twofold axis, as described in previous monomeric IDH structures (Yasutake *et al.*, 2002, 2003; Imabayashi *et al.*, 2006).

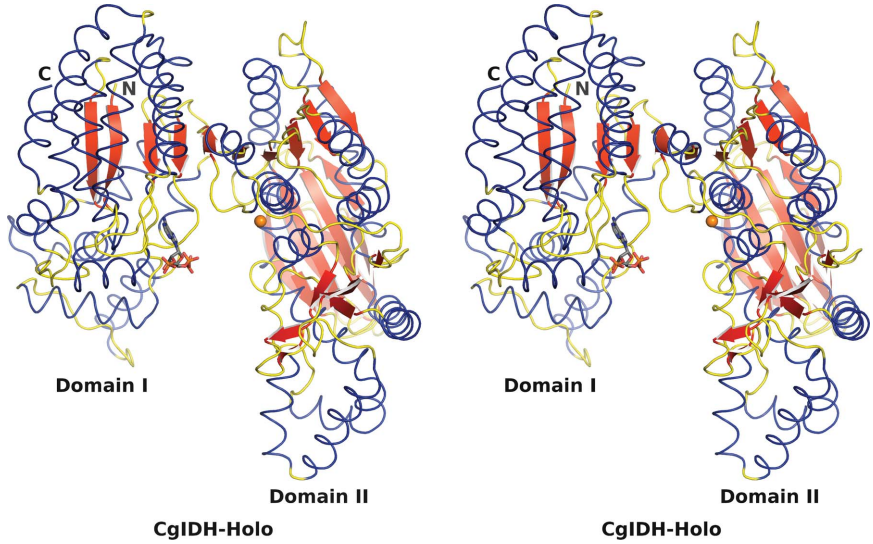

Figure 2
Stereoview of the overall structure of the holoenzyme. CgIDH-Holo consists of a smaller domain I with both N- and C-termini (labelled N and C) and a larger domain II. Secondary-structure elements are colour-coded, showing α-helices (blue), β-strands (red) and loops (yellow). The coenzyme and cofactor bind in their binding sites in the active-site cleft, which is at the interdomain interface, with $NADP^+$ (stick model) in domain I and Mg^{2+} (orange ball) in domain II.

3.3.1. Comparison of CgIDH-Holo with CgIDH-Apo2 and CgIDH-Apo1. CgIDH-Holo and the previously described apoenzyme CgIDH-Apo1 have a very similar open conformation. The interdomain rotation angles of the two forms differ by approximately 1°. The C^{α} atoms of the $NADP^{+}$-binding domains I of the Holo and Apo1 forms can be superimposed on each other with an r.m.s.d. of 0.41 Å (310/313 atoms) and those of the non-$NADP^{+}$-binding domains II with an r.m.s.d. of 0.26 Å (423/425 atoms), as calculated using the program *LSQKAB* (Kabsch, 1976).

In contrast, CgIDH-Apo2 displays an overall conformation that is intermediate between open and closed (Fig. 3). When domains I of the Holo and Apo2 forms in the asymmetric unit are superimposed, the domains II are found to be rotated with respect to each other by an angle of approximately 13°, with residues Glu138 and Gly139 and residues Ser563 and Val564 forming two pairs of mechanical hinges, as determined using the program *DYNDOM* (Hayward & Berendsen, 1998). The N-terminal hinge point is closely flanked by isocitrate-binding residues (as predicted from the AvIDH-Iso structure), as seen in a hypothetical structure with isocitrate–Mn^{2+} modelled in CgIDH-Holo based on a superposition of domains II of CgIDH-Holo and AvIDH-Iso (Fig. 4). Residues Ser563 and Val564 lie at the centre of strand β23 (Leu562–565). The general main-chain hydrogen-bonding pattern between β23 and neighbouring strands does not change on hinge bending. The main-chain amide N atom of Ser563 hydrogen bonds to a water O atom in both molecules in the asymmetric unit since the neighbouring strand β24 ends at Glu575; the main-chain carbonyl O atom of the latter residue also hydrogen bonds to a water in both molecules. In the N-terminal hinge the first position is occupied by Glu138, which is conserved in the monomeric IDH representative sequences (see §2 and Supplementary Material) except in the putative monomeric IDHs from *M. bovis*, *M. tuberculosis* and *Campylobacter jejuni*, in all of which it is replaced by glutamine at the equivalent position. Gly139, on the other hand, is strictly conserved in all representative sequences, as is Ser563 in the first position in the C-terminal hinge. Val564 is replaced by isoleucine in 14 of the 21 sequences, including AvIDH. The C^{α} atoms of domains I of the Holo and Apo2 forms can be superimposed with an r.m.s.d. of 0.43 Å (310/313 atoms) and those of domains II with an r.m.s.d. of 0.39 Å (422/425 atoms).

3.3.2. Comparison of CgIDH and AvIDH structures. Putative isocitrate-binding residues are strictly conserved in the representative monomeric IDH sequences. The CgIDH-Holo domains are open by approximately 24° relative to those

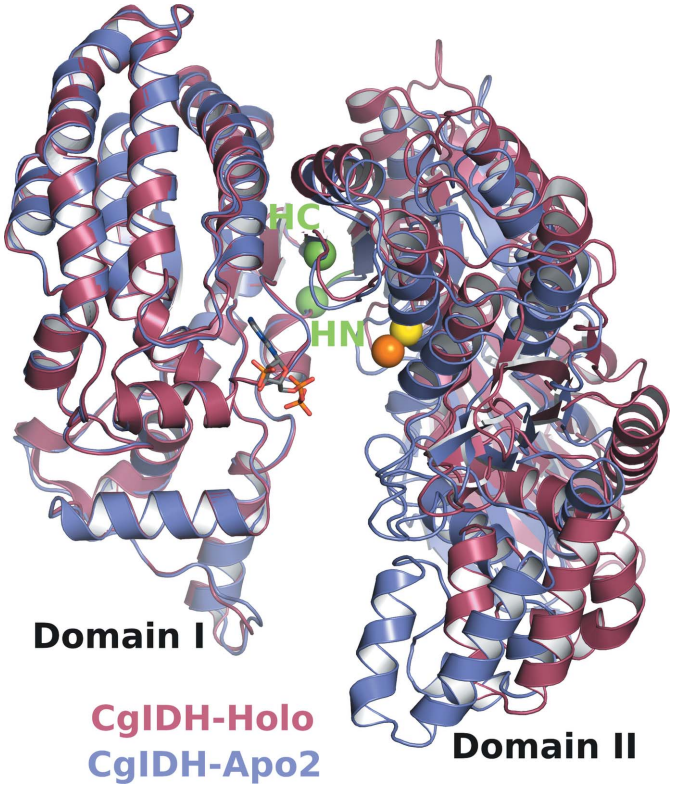

Figure 3
Structural comparison of the holoenzyme and apoenzyme molecules in the asymmetric unit. Domains I of CgIDH-Holo (maroon) and CgIDH-Apo2 (blue) are superimposed, with domains II showing a 13° hinge-bending movement relative to each other, with the locations of the N- and C-terminal hinges (labelled HN and HC, representing Ser138-Gly139 and Ser563-Val564, respectively) coloured green in Cg-Holo and marked by the C^{α} atoms of Ser138 and Ser563 (green balls). Also shown are Mg^{2+} bound to CgIDH-Holo (yellow ball) and CgIDH-Apo2 (orange ball), and $NADP^{+}$ bound to the Holo form (stick model). Hinge points were determined using *DYNDOM* (Hayward & Berendsen, 1998).

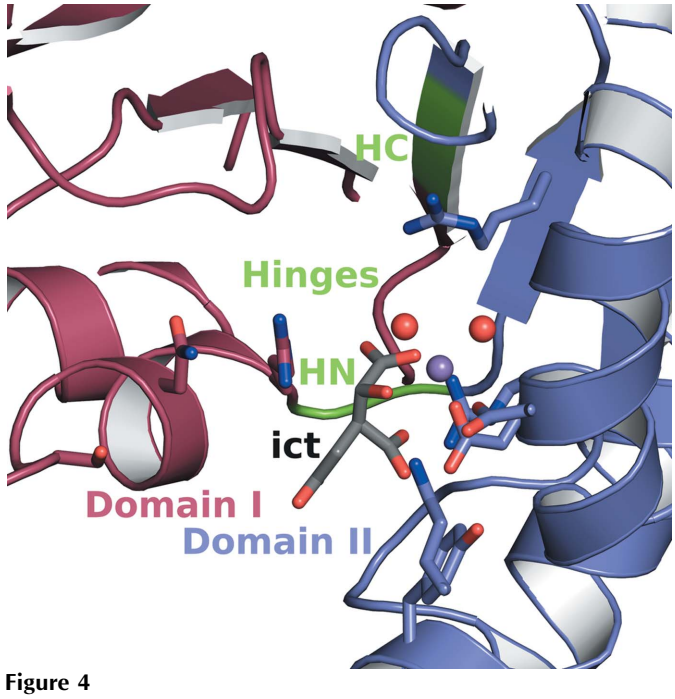

Figure 4
Hypothetical model showing the relationship between hinge points and the isocitrate-binding site. CgIDH-Holo domains I (maroon) and II (blue), showing the N-terminal hinge point (HN; green) in loop α6–β4 and the C-terminal hinge point (HC; green) in strand β23, isocitrate (ict, standard colours), Mn^{2+} (violet ball) and its water oxygen ligands (red balls). Residues predicted to bind the isocitrate–Mn^{2+} complex (stick models, with non-C atoms in standard colours; three in domain I and six in domain II) based on the AvIDH-Iso structure are also shown. Isocitrate coordinates are from PDB entry 1itw (Yasutake *et al.*, 2002) after superposition of its domain II with that of CgIDH-Holo. Hinge points were determined using *DYNDOM* (Hayward & Berendsen, 1998).

of AvIDH-Iso. With domains II of CgIDH-Holo, CgIDH-Apo2 and AvIDH-Iso forms superimposed, marked fraying of the three chains can be seen starting close to the position of the hinges in CgIDH and continuing into domain I (Fig. 5). The fraying is especially prominent at the N-terminal hinge, which falls in a loop, and somewhat less so at the C-terminal hinge, which is part of a β-sheet spanning the two domains. The distance between Mg^{2+} and Mn^{2+} ions bound to CgIDH and AvIDH, respectively, in the superimposed structures is 1.2 Å. The side chains of nine residues make direct binding interactions with isocitrate in AvIDH-Iso (with a distance cutoff of 3.5 Å; Yasutake *et al.*, 2002; PDB entry 1itw). In CgIDH, the putative residues are Ser130, Asn133 and Arg137 in domain I and Arg143, Lys253, Asp346, Tyr416, Arg543 and Asp544 in domain II. The C^{α} atoms of domains I of CgIDH-Holo and AvIDH-Iso can be superimposed on each other with an r.m.s.d. of 0.76 Å (310/313 atoms) and those of domains II with an r.m.s.d. of 1.3 Å (423/425 atoms).

The domains of CgIDH-Holo are rotated by approximately 36° relative to those of AvIDH-Holo (Supplementary Fig. 1). The two holoenzyme molecules are in open and closed conformations, respectively. With domains I of the two holoenzymes superimposed, the distance between the tips of domain II is as large as 33 Å (between C^{α} atoms of residues Leu305 in CgIDH and the conserved equivalent Leu307 in AvIDH). The entry to the isocitrate-binding site is wide in CgIDH-Holo. At one of its narrower points, domains I and II are separated by 11.6 Å (the distance between the C^{β} atoms of Ser130 and Met256) and 4.2 Å (between the C^{β} atoms of the equivalent Ser132 and Met258) in the CgIDH and AvIDH holoenzymes, respectively. C^{α} atoms of domains I of CgIDH-Holo and AvIDH-Holo can be superimposed on each other with an r.m.s.d. of 1.4 Å (310/313 CgIDH atoms) and those of domains II (residues 139–305 and 306–563 in CgIDH overlaid on residues 141–307 and 310–567 in AvIDH, respectively) with an r.m.s.d. of 1.5 Å (423/425 atoms).

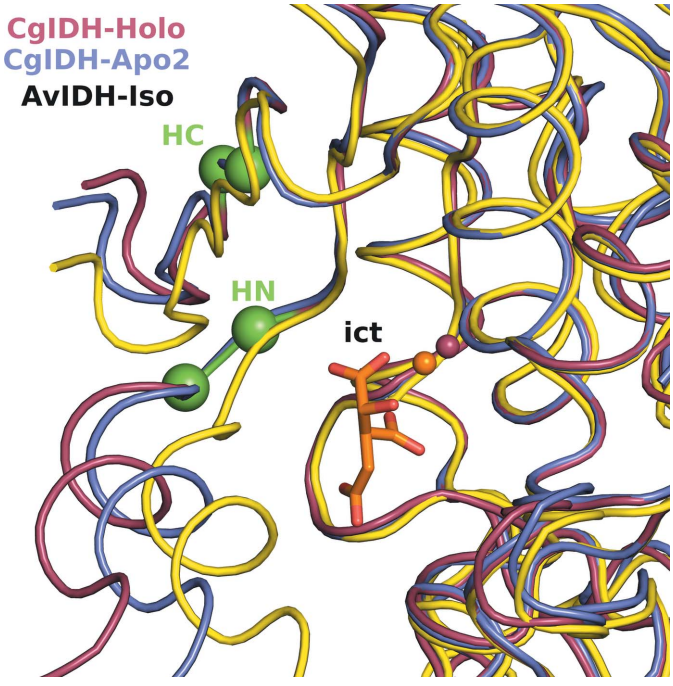

Figure 5
Hinge bending. Domains II of CgIDH-Holo (maroon), CgIDH-Apo2 (blue) and AvIDH-Iso (yellow) were superimposed. Isocitrate (ict; orange and red stick model), Mn^{2+} (orange ball), Mg^{2+} (maroon ball) and the N- and C-terminal hinge points (labelled HN and HC, respectively; green) in loop α6–β4 and strand β23, respectively, are also shown, together with the C^{α} atoms of hinge residues (green balls). AvIDH-Iso coordinates are from PDB entry 1itw (Yasutake *et al.*, 2002). Hinge points were determined using *DYNDOM* (Hayward & Berendsen, 1998).

3.4. $NADP^+$ binding

Fig. 6 shows the electron density in the $NADP^+$-binding site in the interdomain interface, as visible in the $2mF_o - DF_c$ map contoured at the 1.0σ level and OMIT difference density for $NADP^+$ contoured at the 1.75σ level, as calculated before the addition of $NADP^+$ to the model (R_{free} at this point was 3.9% higher than the final value of 22.9%). Electron density corresponding to the adenosine 2′-phosphomonoester 5′-diphosphate moiety of $NADP^+$ was observed. No clear density was observed for nicotinamide and the adjacent ribose, which are not included in the model. The *B* factors of $NADP^+$ atoms are relatively low for the adenine and 2′-phosphate moieties and become progressively higher for the ribose and the diphosphate backbone, with values ranging from 13 $Å^2$ for the N1 N atom of adenine to 71 $Å^2$ for atoms in the distal part of the diphosphate backbone. The N1 nitrogen is hydrogen-bonded to the Asp598 amide N atom, which has a comparable *B* factor of 15 $Å^2$. Values for the coenzyme and neighbouring enzyme atoms are also approximately comparable for the 2′-phosphate moiety. However, protein main-chain atoms in the neighbourhood of the diphosphate moiety have much

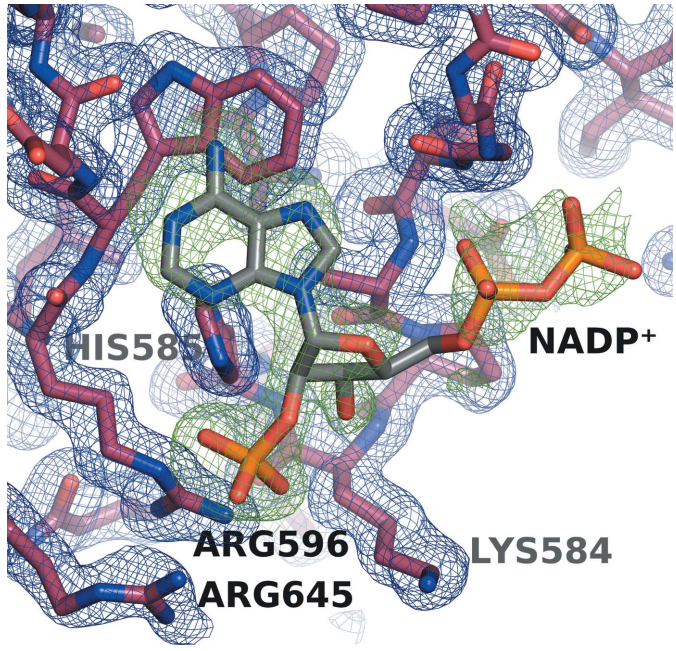

Figure 6
OMIT map. OMIT map $mF_o - DF_c$ difference density (green) contoured at 1.75σ as calculated before the addition of $NADP^+$ to the model and the $2mF_o - DF_c$ map (blue) contoured at the 1.0σ level around protein atoms. The final model is also shown; waters are omitted for clarity.

lower *B* factors (approximately 25 Å^2) compared with the latter (59–71 Å^2). The adenine ring and the endocyclic oxygen of ribose are in the *anti* conformation (Klyne & Prelog, 1960) with respect to each other around the N-glycosidic bond. The furanoid ring of ribose displays approximately a half-chair C3′-*endo*/C2′-*exo* conformation (Sundaralingam, 1969).

The coenzyme is bound to domain I. Direct binding interactions are seen with residues in helix α20 and three surface loops, β24–α20, α20–α21 and α22–α23, namely with Gly580, His585, Arg596, Trp597, Asp598 and Arg645 (Fig. 7). Water-mediated interactions are seen with Thr576, Gly579, Ala582, Lys584, Gly601 and Glu602, the latter two being in helix α21. Coenzyme-binding interactions consist of (i) π-stacking interactions (Hunter & Sanders, 1990) with adenine as part of an aromatic triad, (ii) hydrogen bonding (maximum distance cutoff 3.5 Å) involving N atoms along the edge of adenine opposite the N-glycosidic bond, (iii) specificity-mediating ion pairing and hydrogen bonding between ribose-2′-phosphomonoester and the side chains of four residues and (iv) hydrogen bonding with the ribose and diphosphate backbone of NADP$^+$. Thus, the adenine ring lies at angles of approximately 25° and 85° with respect to the Trp597 and His585 aromatic ring planes, respectively, and the latter two rings at 75° with respect to each other; the centroid of the adenine ring lies in an offset arrangement with respect to the centroids of the Trp597 and His585 rings. The N6 amino N atom of adenine is hydrogen bonded directly to the main-chain carbonyl O atom of Asp598 and indirectly, *via* a differing pair of waters within a five-water network, to the backbone carbonyl O atom of Asp598, the backbone amide N atoms of Gly579 and Gly601 and the side-chain O atoms of Thr576 and Glu602, N1 directly to the main-chain amide N atom of Asp598 and N7 indirectly to the backbone O atom of Gly580. The O3 oxygen of the specific phosphoryl group is hydrogen bonded to His585 N$^{\varepsilon 2}$ and Arg596 N$^{\varepsilon}$, O2 to Arg596 N$^{\eta 2}$ and, through a water, to Lys584 N$^{\zeta}$, and O1 weakly to Arg645 N$^{\eta 2}$. Lys584 and His585 lie on the N-terminal side of helix α20, while Arg596 and Arg645 lie in loops α20–α21 and α22–α23, respectively. The 3′-hydroxyl O atom of ribose is hydrogen bonded *via* a water to the backbone amide N atom of Lys584; in the diphosphate backbone of NADP$^+$ the O1A and O2N O atoms form direct and indirect hydrogen bonds with the backbone amide N atoms of Gly580 and Ala582 in loop β24–α20.

When domains I of the CgIDH-Holo and CgIDH-Apo1 forms are overlaid on each other, the NADP$^+$-binding region superimposes well (Supplementary Fig. 2). In contrast, a similar superimposition of the CgIDH-Holo and CgIDH-Apo2 forms (Supplementary Fig. 3) shows that, although the two molecules superimpose relatively well in this region generally, there are significant differences in the environments of the side chains of Apo2 residues Arg596 and Arg645, both of which form ion pairs with the 2′-phosphate group of NADP$^+$ in the Holo form. Firstly, the side-chain carboxylate of Asp506 of a symmetry-neighbour molecule forms a double hydrogen bond with the side chain of Apo2 Arg596. Both side chains are in fair electron density. Secondly, the side chain of Arg645 of Apo2 points into a region of space that would be occupied by the 2′-phosphate of a bound NADP$^+$. Thirdly, the side chain of Glu508 of the symmetry neighbour of Apo2 is disordered but potentially within good hydrogen-bonding distance of the side-chain NH1 and NH2 N atoms of Arg645 and the NH2 N atom of Arg596. The symmetry-related neighbour of the Holo form, on the other hand, is appreciably more distant from the NADP$^+$-binding site.

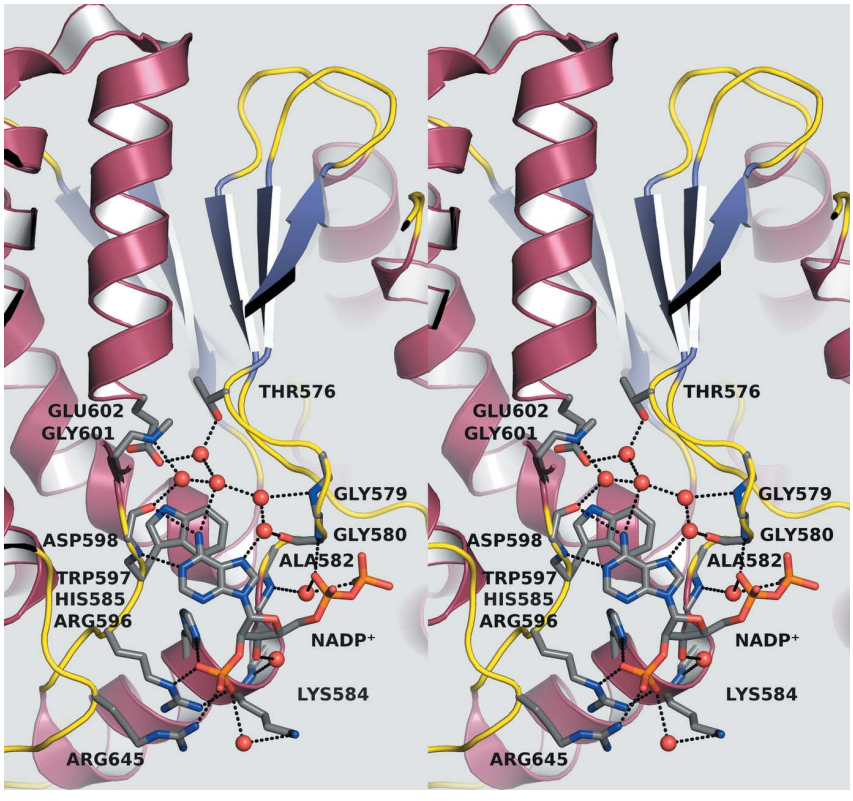

Figure 7
Stereoview of NADP$^+$-binding interactions in CgIDH-Holo. Protein residues (stick model) and waters (red balls) involved in binding NADP$^+$ are shown, together with the secondary-structure context, with α-helices shown in maroon, β-strands in blue, loops in yellow and potential hydrogen bonds as black dashes. Part of the α-helix cartoon in the Glu602 region is absent for clarity.

3.5. Mg^{2+} binding

Putative Mg^{2+}-binding and Mn^{2+}-binding residues are strictly conserved in the 21 representative monomeric IDH sequences. CgIDH-Holo and CgIDH-Apo2 each have an Mg^{2+} ion hexacoordinated in an approximate octahedral geometry to oxygen ligands of the following helix α14 and α19 aspartate resi-

dues of domain II: bidentate binding to the backbone carbonyl O atom and side-chain carboxylate $O^{\delta2}$ of Asp544, the side-chain carboxylate $O^{\delta2}$ and $O^{\delta1}$, respectively, of Asp346 and Asp548, and two water O atoms. Structural comparison of AvIDH-Iso and CgIDH-Holo suggests that upon isocitrate binding in the latter the ligands of Mg^{2+} change such that the O2 and O7 O atoms of isocitrate replace water O atoms wat1109 and wat1110 (numbering as in CgIDH-Holo), respectively, while a water O atom replaces the backbone carbonyl O of Asp544 and the side-chain carboxylate $O^{\delta1}$ of Asp548; the $O^{\delta2}$ O atoms of Asp346 and Asp544 are preserved in their respective positions.

4. Discussion

This study reports a 1.9 Å resolution crystal structure of CgIDH cocrystallized with its coenzyme $NADP^+$ and cofactor Mg^{2+}. An Mg^{2+} ion is bound to each of the two CgIDH molecules in the asymmetric unit. Electron density for approximately two thirds of the coenzyme $NADP^+$ molecule is found in the predicted binding site of one of the two CgIDH molecules, with the other molecule being in the $NADP^+$-free apoenzyme form. The $NADP^+$-bound CgIDH is in an open conformation. A hinge bending, which has been previously suggested to occur in monomeric IDHs (Yasutake *et al.*, 2003; Imabayashi *et al.*, 2006), of 13° is seen between the two molecules in the asymmetric unit within the same crystal. Two hinge points are identified, one of which is closely flanked by the substrate-binding site. Finally, disruption of coenzyme binding in one of the enzyme molecules in the asymmetric unit is observed.

4.1. Overall structure

The present structure has the same space group, *C*2, and a similar solvent content, as the previous CgIDH apoenzyme structure (Imabayashi *et al.*, 2006; PDB entry 2b0t). However, there are two molecules in the asymmetric unit in the former compared with one in the latter. The doubling of the unit-cell volume is achieved by an approximate doubling of the unit-cell dimension *c* (236.4 Å compared with 124.0 Å).

In a previous study, a change in fluorescence intensity upon the addition of $NADP^+$ to CgIDH in solution suggested a conformational change upon $NADP^+$ binding (Imabayashi *et al.*, 2006). The present structure is partly inconsistent with this result: although the Holo form displays a 13° hinge-bending movement relative to the Apo2 form in the same asymmetric unit, the former is in a closely similar overall conformation compared with the Apo1 form from the previous structure under relatively similar conditions. Potentially, part of the similarity between the Apo1 and Holo forms could be a consequence of model bias since Apo1 was used as the search model in molecular replacement in the present study. However, the Apo1 and Apo2 forms differ by a 13° hinge-bending movement relative to each other, suggesting that the Holo and Apo1 forms are more similar to each other in overall conformation compared with the two Apo forms despite the potential model bias. Significant but chemically reasonable differences in the $NADP^+$-binding regions in the Holo and Apo2 forms in the current structure give additional confidence in the above interpretation. Also, part of domain II of each molecule in the asymmetric unit is inserted into the interdomain cleft of the other (Fig. 1). This suggests that crystal packing may have a significant effect on the overall conformation of CgIDH. A similar conclusion was made for AvIDH-Holo (discussed below) as well as (based on a comparison of crystal structures with results from small-angle X-ray scattering) for the IDH-related dimeric IPMDH from *Thermus thermophilus* (Kadono *et al.*, 1995).

4.2. Hinge bending

In CgIDH and AvIDH, the N-terminal part of the protein chain forms part of domain I and then crosses over to form the entire domain II before returning back to form the rest of domain I. Thus, two hinges at the interdomain boundary may be expected. Hinge movements in AvIDH-Holo relative to AvIDH-Iso from a different crystal were focused in 11 residues from three groups in two loop regions (residues 137–138, 142–144 and 560–565; AvIDH numbering; Yasutake *et al.*, 2003). Since isocitrate bound to residues in both domains, it was pointed out that it could play a role in fixing the two domains. In the present study, the Holo and Apo2 forms in the asymmetric unit show an approximately 13° rigid-body hinge-bending movement relative to each other. Two pairs of two-residue hinges that lie in loop $\alpha6$–$\beta4$ (residues Glu138-Gly139; CgIDH numbering) and in the middle of strand $\beta23$ (Ser563-Val564) were identified using the program *DYNDOM* (Hayward & Berendsen, 1998). The latter strand is one of the central pair of strands in the ten-stranded β-sheet that weaves through the two domains. Hinge bending is not accompanied by disruption or acquisition of hydrogen bonds made by the strand. Since both molecules are in the same crystal, conformational changes arising from differences in solution conditions are minimized, albeit not eliminated owing to the dissimilar environment of the two molecules within the asymmetric unit, suggesting that the hinges determined may reflect an intrinsic property of CgIDH dynamics under a given set of conditions. Structural and structure-based sequence comparisons between AvIDH-Iso and CgIDH-Holo suggest that, as in AvIDH, isocitrate binds to CgIDH residues in both domains. The Glu138-Gly139 hinge is tightly flanked on both sides, in sequence and three-dimensional structure, by putative isocitrate-binding residues Ser130, Asn133 and, especially, Arg137 in domain I and Arg143 in domain II. This suggests a model in which the isocitrate-binding site is positioned such that small structural changes induced by the binding of a relatively small ligand to both sides of, and in intimate proximity to, a mechanical hinge can be converted into large-scale overall conformational changes of the molecule. This can presumably be seen between CgIDH-Holo and AvIDH-Iso, with the two molecules displaying a 24° hinge-bending movement relative to each other, with AvIDH-Iso in a more closed conformation. Four different conformations of mono-

meric IDHs have been observed to date in four structures, with a difference of 9–13° in hinge movement between them, further confirming suggestions by Yasutake *et al.* (2003) and Imabayashi *et al.* (2006) that monomeric IDHs are flexible molecules with a low free-energy barrier between conformational states. Hinge movements have also been described in other proteins (reviewed in Gerstein *et al.*, 1994), including the dimeric IDHs EcIDH (Finer-Moore *et al.*, 1997; Doyle *et al.*, 2001), IDH from *Bacillus subtilis* (BsIDH; Singh *et al.*, 2001), HcIDH (Xu *et al.*, 2004), ApIDH (Karlstrom *et al.*, 2005) and ScIDH (Peng *et al.*, 2008). In EcIDH, hinge movement has been described in β-strand *F*, which lies at the centre of the 12-stranded β-sheet that runs through the two domains in that protein; it involves no rearrangement of hydrogen bonds in the sheet (Finer-Moore *et al.*, 1997).

4.3. Active-site access

In the only previously available holoenzyme structure of a monomeric IDH, AvIDH-Holo, insufficient space was reported for isocitrate binding in the active site, access to which was blocked by $NADP^+$ bound to a closed, apparently inactive, conformation of the enzyme (Yasutake *et al.*, 2003; PDB entry 1j1w). It was suggested that the flexible molecule had adopted a closed conformation owing to crystal lattice forces. Kinetic data for AvIDH also indicated that the binding of the first substrate does not influence the binding of the second in the random order in the forward direction (Wicken *et al.*, 1972). Similarly, in EcIDH binding of $NADP^+$ causes little change in the K_m for isocitrate (Dean & Koshland, 1993). In the present structure, CgIDH-Holo displays an open-conformation complex with $NADP^+$. In comparison with AvIDH-Holo, a wide 36° hinge-opening movement is seen. The isocitrate-binding site is accessible to isocitrate. Given the apparent flexibility of the molecule, the form observed may represent a physiologically relevant conformation of the molecule. However, the putative isocitrate-binding residues are too far apart to bind isocitrate in the open conformations seen in CgIDH structures. Isocitrate binding favours a closed conformation, which is also presumably the catalytically active conformation, similar to that seen in the AvIDH-Iso structure. Thus, the AvIDH and CgIDH structures complement each other in providing a fuller picture of coenzyme and substrate binding in monomeric IDHs. The conformation seen in CgIDH-Apo2 has an intermediate hinge-bending angle between the open forms of CgIDH on the one hand and the closed AvIDH-Iso on the other. The structures imply a significant conformational change upon isocitrate binding, which is consistent with the fluorescence changes observed in CgIDH upon isocitrate binding (Imabayashi *et al.*, 2006). The crystal structures may thus be sampling conformations on a functionally relevant trajectory.

4.4. Possible implications for regulation and disease

As discussed above, monomeric IDHs appear to display a high degree of intrinsic flexibility in general and implied conformational change upon isocitrate binding in particular. Concerted competitive inhibition with respect to isocitrate by glyoxylate and oxaloacetate in IDHs (Shiio & Ozaki, 1968) and concerted inhibition in several monomeric IDHs (Ochiai *et al.*, 1979; Leyland & Kelly, 1991; Eikmanns *et al.*, 1995) has been reported. The high conservation of isocitrate-binding and divalent metal-binding residues between the dimeric and monomeric IDHs (Yasutake *et al.*, 2002) suggests that the inhibition in monomeric IDHs could also be competitive with respect to isocitrate, possibly involving a similar mechanism as for isocitrate, with attendant hinge bending. Owing to the large 24° interdomain hinge rotation observed between CgIDH-Apo1 and CgIDH-Holo on the one hand and AvIDH-Iso on the other, this hypothesis could be testable using small-angle X-ray scattering in solution (SAXS). Banerjee *et al.* (2004) have suggested that IDHs from *M. tuberculosis* could potentially serve as drug targets against TB, a leading cause of mortality from infectious diseases. Further research into concerted inhibition by glyoxylate and oxaloacetate may be helpful in this effort.

4.5. $NADP^+$ binding

Overall, direct $NADP^+$-binding interactions are seen in one α-helix and three loops in CgIDH, as distinct from the typical $\beta\alpha\beta\alpha\beta$ motif of the Rossmann fold (Rossmann *et al.*, 1974). All residues which form binding interactions with $NADP^+$ in the form of direct hydrogen bonds or salt bridges and π-stacking interactions are strictly conserved in characterized monomeric IDHs from *A. vinelandii*, *C. maris*, *R. vannielii*, *V. parahaemolyticus* and *C. glutamicum*. CgIDH residues that form indirect water-mediated hydrogen bonds with $NADP^+$ are also strictly conserved in these monomeric IDHs, but this may be less significant as there is a high background of sequence homology amongst monomeric IDHs in general: CgIDH shares a sequence identity and a similarity of 57–62% and 76–81%, respectively, with monomeric IDHs from these organisms.

The adenine ring of $NADP^+$ is involved in π-stacking interactions (Hunter & Sanders, 1990). The adenine and Trp597 rings appear to interact mainly in an offset π-stacked arrangement, with an additional T-shaped (edge-on) component; the aromatic ring of His585 interacts in an approximately T-shaped arrangement with respect to both the adenine and Trp597 rings. The stacking interactions observed thus appear to be dominated by attractive geometries. Highly conserved hydrogen bonds are formed between the N6 and N1 N atoms of adenine and the main-chain carbonyl O atom and amide N atom, respectively, of Asp598. $NADP^+$-binding interactions in AvIDH and CgIDH holoenzymes are in general similar in the adenosine part of the coenzyme; among the differences, a network of water-mediated hydrogen bonds is observed between the adenine ring and the protein in the higher resolution structure of the CgIDH holoenzyme (1.9 Å compared with 3.2 Å). In comparison with the adenosine moiety, the diphosphate forms significantly fewer interactions with the protein, which is in general similar to observations in AvIDH-Holo, where the diphosphate was not found to interact with

the main chain (Yasutake *et al.*, 2003), and in EcIDH, where only one hydrogen bond was observed between the proximal phosphate and Gly340 N (Bolduc *et al.*, 1995; PDB entry 1ide).

4.5.1. $NADP^+$ specificity. In CgIDH, well ordered side chains of His585, Arg596 and Arg645 interact with the 2′-phosphate group of the adenosine ribose of $NADP^+$ directly, forming hydrogen bonds and ion pairs. In addition, an ordered side chain of Lys584 makes a water-mediated hydrogen bond with the phosphate group. Two of these residues, His585 and Lys584, are on the N-terminal side of helix α20 and apparently utilize the dipole moment of the helix to bind the phosphate (Wierenga *et al.*, 1985). The binding interactions seen confirm a prediction made by Chen & Yang (2000) that Lys584 and His585 interact with the 2′-phosphate group of $NADP^+$. His585, Arg596 and Arg645 are highly conserved in the sequences of representative IDHs, with two exceptions. In the putative monomeric IDH from *Ralstonia eutropha* (ReIDH), Arg645 is replaced by Pro652 at the equivalent position. Since this arginine appears to be a significant determinant of coenzyme specificity, this switch, if uncompensated for, may significantly affect $NADP^+$ specificity and/or activity in ReIDH. Indeed, heterologous expression of ReIDH in *E. coli* has been reported to lead to a gene product devoid of IDH activity (Wang *et al.*, 2003). An NCBI database search revealed that all four putative monomeric ReIDH sequences reported for *R. eutropha* contain a proline residue at the position equivalent to that of Arg645 in CgIDH. Although suggestive, it is unclear whether this R652P switch in ReIDH is the cause of the observed loss of activity. In *C. jejuni* IDH, the position equivalent to His585 in CgIDH is occupied by Gln580. The impact of this change is unclear.

In EcIDH, the major determinants of $NADP^+$ specificity are Arg395, Tyr345, Tyr391 and Arg292′ (from the second subunit; Hurley *et al.*, 1991; Chen *et al.*, 1995). In general terms, two main differences in coenzyme binding seem to stand out on going from EcIDH to the CgIDH holoenzyme: (i) two O atoms (of Tyr side chains) that interact with the 2′-phosphate in EcIDH are replaced in CgIDH by directly and indirectly interacting N atoms (of His and Lys side chains, respectively) that can potentially bear a positive charge and (ii) π-stacking interactions with a His residue in EcIDH are rearranged around the adenine and a Trp residue is added in place of a Val and an Ile, forming space for water-mediated hydrogen bonds between the adenine and the protein in CgIDH. If these differences between the two holoenzymes are excluded, the remainder of the interactions are remarkable for their general residue similarity, with structurally approximately equivalent residues in the general coenzyme-binding region being Arg395/Arg596, Arg292′/Arg645, Gly340/Gly580, Ala342/Ala582 and Lys344/Lys584 in EcIDH and CgIDH, respectively, apparently supporting the hypothesis of a divergent evolution of the two IDHs suggested by Chen & Yang (2000). However, the significance of the differences in coenzyme binding between EcIDH and CgIDH is not obvious. Thus, almost all of the residues interacting with $NADP^+$, especially the three conserved residues directly interacting with the 2′-phosphate, are also highly conserved in monomeric IDH from *R. vannielii* (RvIDH), which prefers $NADP^+$ by a factor of only 400 (Leyland & Kelly, 1991) compared with a factor of 7000 in EcIDH. Hence, other factors are likely to play a significant role in determining specificity. These factors may include 'second-layer' residues (Hurley *et al.*, 1996), which only interact with the 2′-phosphate indirectly *via* the directly interacting 'first-layer' residues, longer range interactions (Chen *et al.*, 1997) and dynamics. The second-layer residue Lys584 in CgIDH is conservatively replaced by Arg591 at the equivalent position in RvIDH. In the absence of a structure, it is difficult to judge the significance of this substitution.

In the closed and open forms of the AvIDH and CgIDH holoenzymes, equivalent residues interact with the 2′-phosphate: thus, the specificity-mediating interactions observed in the closed form are already present in the open form of CgIDH, suggesting that specific recognition of $NADP^+$ occurs as an early step in this enzyme. Residues from a single domain are positioned such that both access and binding are achievable, which is consistent with its combination of specificity and performance. This appears to contrast to a certain degree with some dimeric IDHs. Thus, in HcIDH (Xu *et al.*, 2004) three residues (a His, a Gln and a Lys) interact directly with the 2′-phosphate in the closed form (PDB entry 1t0l), while two, including one that does not interact in the closed form, do so in the open form (an Arg and a His; PDB entry 1t09); in ApIDH, the equivalent numbers are four interacting residues (Arg, Lys, Gln and Tyr; PDB entry 1xkd, chain *B*) in the closed conformation and two (Arg and Tyr; chain *A*) in the open conformation (Karlstrom *et al.*, 2005).

4.5.2. Nicotinamide-binding mode and order/disorder. An ordered $NADP^+$ molecule has been observed in many IDH and related structures. In AvIDH-Holo, it was suggested that the protein fixed the nicotinamide mononucleotide moiety in place even in the absence of isocitrate; after isocitrate binding the reaction could take place immediately (Yasutake *et al.*, 2003). This appeared to be consistent with the high turnover number of AvIDH, which has been reported as 930 s^{-1} (310 K; Barrera & Jurtshuk, 1970) and 250 s^{-1} (298 K; Wicken *et al.*, 1972), compared with 87 and 81 s^{-1} for CgIDH and EcIDH, respectively (294 K; Chen & Yang, 2000). Nicotinamide binding by the protein itself (Glu87) has also been suggested in IPMDH from *T. thermophilus* (Dean & Dvorak, 1995). In EcIDH, on the other hand, clear electron density was observed for the entire $NADP^+$ molecule in the presence of isocitrate (Stoddard *et al.*, 1993; Bolduc *et al.*, 1995). In its absence, the nicotinamide nucleotide of $NADP^+$, with or without the second 5′-phosphate, was disordered in wild-type (PDB entries 9icd and 1bl5; Hurley *et al.*, 1991; Stoddard & Koshland, 1993; Stoddard *et al.*, 1998) and mutant EcIDH (PDB entry 1iso; Bolduc *et al.*, 1995; Hurley *et al.*, 1996). In this case, the γ-carboxylate of isocitrate was stabilized by a crucial hydrogen bond to Ser113 (Dean *et al.*, 1996) and formed the binding site for the positively charged nicotinamide (PDB entry 1ide; Bolduc *et al.*, 1995), apparently aligning it during hydride transfer. Chen & Yang (2000) found that CgIDH and EcIDH displayed relatively similar substrate-specificity profiles with substrates differing in the substituent at the γ

position in isocitrate, but CgIDH was an order of magnitude more specific for isocitrate compared with EcIDH. This suggested that the γ-carboxylate of isocitrate also forms the binding site for the nicotinamide ring in CgIDH; in the absence of isocitrate the nicotinamide nucleotide might be expected to be disordered.

In the absence of isocitrate, no clear density corresponding to the nicotinamide nucleoside moiety of $NADP^+$ was observed in the present structure. At high pH (below pH 14), the decomposition of NAD^+ mainly involves base-catalyzed chemical hydrolysis of the N-glycosidic bond, producing adenosine diphosphate ribose (ADP-ribose) and nicotinamide (Oppenheimer, 1987). The rate displays a direct pH dependence from pH 9 to 11.5, with residual pH-independent hydrolysis occurring at a low constant rate (at constant temperature) from pH 2 to 7 (Lowry *et al*., 1961). In AvIDH-Holo, electron density for the entire $NADP^+$ molecule was observed under crystallization conditions (pH 7.0, 291 K, crystal growth within one month) that were similar to those in the present study (pH 7.3, 295 K, crystal growth within five weeks). Some difference in the degree of nicotinamide hydrolysis in the two experiments could still be present owing to differences in temperature and the type and concentration of salt (Lowry *et al*., 1961). Tris buffer (used in the present study) does not increase the hydrolysis rate (Anderson & Anderson, 1963). Taken together, partial hydrolysis of nicotinamide in the approximately pH-independent regime is presumed and the ribose adjoining the nicotinamide is assumed to be disordered. However, CgIDH-Holo in general and the 2′-phosphoadenosine moiety of $NADP^+$ together with the binding residues in particular are in well ordered density, make chemical sense and are largely consistent with many previous IDH structures. Thus, it is unlikely that the observed structure has been significantly affected by the possible hydrolysis of nicotinamide. Furthermore, in EcIDH the position of the adenosyl ring of $NADP^+$ with respect to the binding site was found to be unchanged when the entire $NADP^+$ molecule was ordered compared with that when the nicotinamide nucleotide was disordered (Bolduc *et al.*, 1995; PDB entry 1ide). In the absence of isocitrate, $NADP^+$ bound to EcIDH owing to the affinity of its adenine moiety (Stoddard *et al.*, 1993); the adenosyl-ribose groups, especially including the 2′-phosphate, of $NADP^+$ or NADPH were found to be the main binding determinants (Stoddard *et al.*, 1998). This suggests that disorder in the nicotinamide nucleoside moiety may not significantly affect the coenzyme-binding interactions seen in the CgIDH holoenzyme. It is also possible that the marked solvent exposure of the ligand in an open conformation of the enzyme has led to disorder.

4.5.3. Two models for active-site access in IDH holoenzymes. In EcIDH, the disorder in the nicotinamide nucleotide moiety in the absence of the substrate (Hurley *et al.*, 1991) appeared to play a role in making the active site accessible to the substrate when $NADP^+$ bound first (Stoddard *et al.*, 1993) in the random-order addition of substrate and coenzyme (Dean & Koshland, 1993). The CgIDH-Holo structure suggests that in this enzyme, and possibly in monomeric IDHs in general, substrate access to the active site may not be limited by an ordered $NADP^+$ when it binds first (assuming a random-order substrate and coenzyme addition model in the forward direction, as in AvIDH; Wicken *et al.*, 1972). The large hinge bending appears to facilitate substrate access to the active site in CgIDH. It is conceivable that hinge bending allows a degree of diversification in monomeric IDHs with respect to the mode of nicotinamide binding and, possibly, substrate specificity. The protein itself could bind nicotinamide in the absence of isocitrate in AvIDH. In CgIDH the γ-carboxylate of the bound isocitrate could also be involved, as in EcIDH.

4.5.4. Apoenzyme in the asymmetric unit. A trivial reason for $NADP^+$ binding to only one of the two enzyme molecules in the asymmetric unit could be that the coenzyme concentration was too low. This appears to be unlikely: the K_m of CgIDH with respect to $NADP^+$ has been determined to be between 4 μM (Chen & Yang, 2000) and 24 μM (Eikmanns *et al.*, 1995), whereas the concentration of $NADP^+$ used in the crystallization conditions was 10 mM. In the Apo2 form, the side chains of the negatively charged Asp506 and Glu508 from a symmetry-related molecule are present in close proximity to the positively charged side chains of Arg596 and Arg645, which are two of the three residues that directly bind the negatively charged 2′-phosphate moiety of $NADP^+$ in the holoenzyme (Supplementary Fig. 3). Asp506 makes an ordered salt bridge with Arg596. Glu508 is presumed to be disordered. It is well within hydrogen-bonding distance of the side chains of both arginines, especially Arg645, and apparently interacts with them. Thus, although unintended, the symmetry-related interactions appear to mimic the crystallographic equivalent of a genetic mutagenesis experiment, with electrostatic competition for positively charged binding residues abolishing coenzyme binding.

We thank Professor Bernhard Eikmanns, University of Ulm, Germany for the generous gift of the CgIDH gene, Fumie Imabayashi for the purified protein, Dr Sanjukta Aich and Yvonne Leduc for practical suggestions, Dr Pawel Grochulski for help with data collection, Drs Andrea Thorn and Lata Prasad for helpful suggestions on refinement, Drs Tim Grüne and Tobias Beck for critical comments on the manuscript and Dr Christian Hübschle and Julian Holstein for useful advice. NSS thanks the College of Medicine and Department of Biochemistry, University of Saskatchewan, Canada, for graduate fellowships and scholarships, respectively, and the Faculty of Chemistry, University of Göttingen, Germany for further support. A grant to LTJD by the National Sciences and Engineering Research Council, Canada is gratefully acknowledged.

References

Anderson, B. M. & Anderson, C. D. (1963). *J. Biol. Chem.* **238**, 1475–1478.

Audette, G. F., Quail, J. W., Hayakawa, K., Bai, C., Chen, R. D. & Delbaere, L. T. J. (1999). *Acta Cryst.* D**55**, 1584–1585.

Bai, C., Fernandez, E., Yang, H. & Chen, R. (1999). *Protein Expr. Purif.* **15**, 344–348.

Banerjee, S., Nandyala, A., Podili, R., Katoch, V. M., Murthy, K. J. R. & Hasnain, S. E. (2004). *Proc. Natl Acad. Sci. USA*, **101**, 12652–12657.

Barrera, C. R. & Jurtshuk, P. (1970). *Biochim. Biophys. Acta*, **220**, 416–429.

Bolduc, J. M., Dyer, D. H., Scott, W. G., Singer, P., Sweet, R. M., Koshland, D. E. Jr & Stoddard, B. L. (1995). *Science*, **268**, 1312–1318.

Brünger, A. T. (1992). *Nature (London)*, **355**, 472–475.

Chen, R. & Gadal, P. (1990). *Plant Physiol. Biochem.* **28**, 411–427.

Chen, R., Greer, A. & Dean, A. M. (1995). *Proc. Natl Acad. Sci. USA*, **92**, 11666–11670.

Chen, R., Greer, A. F. & Dean, A. M. (1997). *Eur. J. Biochem.* **250**, 578–582.

Chen, R. & Yang, H. (2000). *Arch. Biochem. Biophys.* **383**, 238–245.

Chen, V. B., Arendall, W. B., Headd, J. J., Keedy, D. A., Immormino, R. M., Kapral, G. J., Murray, L. W., Richardson, J. S. & Richardson, D. C. (2010). *Acta Cryst.* D**66**, 12–21.

Chung, A. E. & Franzen, J. S. (1969). *Biochemistry*, **8**, 3175–3184.

Dang, L. *et al.* (2009). *Nature (London)*, **462**, 739–744.

Davis, I. W., Leaver-Fay, A., Chen, V. B., Block, J. N., Kapral, G. J., Wang, X., Murray, L. W., Arendall, W. B. III, Snoeyink, J., Richardson, J. S. & Richardson, D. C. (2007). *Nucleic Acids Res.* **35**, W375–W383.

Dean, A. M. & Dvorak, L. (1995). *Protein Sci.* **4**, 2156–2167.

Dean, A. M. & Golding, G. B. (1997). *Proc. Natl Acad. Sci. USA*, **94**, 3104–3109.

Dean, A. M. & Koshland, D. E. Jr (1993). *Biochemistry*, **32**, 9302–9309.

Dean, A. M., Shiau, A. K. & Koshland, D. E. Jr (1996). *Protein Sci.* **5**, 341–347.

Doyle, S. A., Beernink, P. T. & Koshland, D. E. Jr (2001). *Biochemistry*, **40**, 4234–4241.

DeLano, W. L. (2002). *PyMOL*. http://www.pymol.org.

Eikmanns, B. J., Rittmann, D. & Sahm, H. (1995). *J. Bacteriol.* **177**, 774–782.

Emsley, P., Lohkamp, B., Scott, W. G. & Cowtan, K. (2010). *Acta Cryst.* D**66**, 486–501.

Finer-Moore, J., Tsutakawa, S. E., Cherbavaz, D. B., LaPorte, D. C., Koshland, D. E. Jr & Stroud, R. M. (1997). *Biochemistry*, **36**, 13890–13896.

Florio, W., Bottai, D., Batoni, G., Esin, S., Pardini, M., Maisetta, G. & Campa, M. (2002). *Clin. Diagn. Lab. Immunol.* **9**, 846–851.

Fukunaga, N., Imagawa, S., Sahara, T., Ishii, A. & Suzuki, M. (1992). *J. Biochem.* **112**, 849–855.

Garnak, M. & Reeves, H. C. (1979). *Science*, **203**, 1111–1112.

Gerstein, M., Lesk, A. M. & Chothia, C. (1994). *Biochemistry*, **33**, 6739–6749.

Gerstmeir, R., Wendisch, V. F., Schnicke, S., Ruan, H., Farwick, M., Reinscheid, D. & Eikmanns, B. J. (2003). *J. Biotechnol.* **104**, 99–122.

Hayward, S. & Berendsen, H. J. C. (1998). *Proteins*, **30**, 144–154.

Howlin, B., Butler, S. A., Moss, D. S., Harris, G. W. & Driessen, H. P. C. (1993). *J. Appl. Cryst.* **26**, 622–624.

Hunter, C. A. & Sanders, J. K. M. (1990). *J. Am. Chem. Soc.* **112**, 5525–5534.

Hurley, J. H., Chen, R. & Dean, A. M. (1996). *Biochemistry*, **35**, 5670–5678.

Hurley, J. H., Dean, A. M., Sohl, J. L., Koshland, D. E. Jr & Stroud, R. M. (1990). *Science*, **249**, 1012–1016.

Hurley, J. H., Dean, A. M., Koshland, D. E. Jr & Stroud, R. M. (1991). *Biochemistry*, **30**, 8671–8678.

Hurley, J. H., Thorsness, P. E., Ramalingam, V., Helmers, N. H., Koshland, D. E. Jr & Stroud, R. M. (1989). *Proc. Natl Acad. Sci. USA*, **86**, 8635–8639.

Imada, K., Sato, M., Tanaka, N., Katsube, Y., Matsuura, Y. & Oshima, T. (1991). *J. Mol. Biol.* **222**, 725–738.

Imada, K., Tamura, T., Takenaka, R., Kobayashi, I., Namba, K. & Inagaki, K. (2008). *Proteins*, **70**, 63–71.

Imabayashi, F., Aich, S., Prasad, L. & Delbaere, L. T. J. (2006). *Proteins*, **63**, 100–112.

Ishii, A., Ochiai, T., Imagawa, S., Fukunaga, N., Sasaki, S., Minowa, O., Mizuno, Y. & Shiokawa, H. (1987). *J. Biochem.* **102**, 1489–1498.

Kabsch, W. (1976). *Acta Cryst.* A**32**, 922–923.

Kabsch, W. (2010). *Acta Cryst.* D**66**, 125–132.

Kabsch, W. & Sander, C. (1983). *Biopolymers*, **22**, 2577–2637.

Kadono, S., Sakurai, M., Moriyama, H., Sato, M., Hayashi, Y., Oshima, T. & Tanaka, N. (1995). *J. Biochem.* **118**, 745–752.

Karlstrom, M., Stokke, R., Steen, I. H., Birkeland, N. K. & Ladenstein, R. (2005). *J. Mol. Biol.* **345**, 559–577.

Klyne, W. & Prelog, V. (1960). *Experientia*, **16**, 521–523.

Kornberg, H. L. (1966). *Biochem. J.* **99**, 1–11.

Kornberg, H. L. & Krebs, H. A. (1957). *Nature (London)*, **179**, 988–991.

Krebs, H. A. & Johnson, W. A. (1937). *Enzymologia*, **4**, 148–156.

LaPorte, D. C. & Koshland, D. E. Jr (1982). *Nature (London)*, **300**, 458–460.

Leyland, M. L. & Kelly, D. J. (1991). *Eur. J. Biochem.* **202**, 85–93.

Lovell, S. C., Davis, I. W., Arendall, W. B., de Bakker, P. I. W., Word, J. M., Prisant, M. G., Richardson, J. S. & Richardson, D. C. (2002). *Proteins*, **50**, 437–450.

Lowry, O. H., Passonneau, J. V. & Rock, M. K. (1961). *J. Biol. Chem.* **236**, 2756–2759.

Madsen, D., Johansson, P. & Kleywegt, G. J. (2002). *Indonesia*. http://xray.bmc.uu.se/dennis/.

McCoy, A. J., Grosse-Kunstleve, R. W., Adams, P. D., Winn, M. D., Storoni, L. C. & Read, R. J. (2007). *J. Appl. Cryst.* **40**, 658–674.

McKinney, J. D., zu Bentrup, K. H., Muñoz-Elías, E. J., Miczak, A., Chen, B., Chan, W., Swenson, D., Sacchettinik, J. C., Jacobs, W. R. Jr & Russell, D. G. (2000). *Nature (London)*, **406**, 735–738.

Mesecar, A. D., Stoddard, B. L. & Koshland, D. E. Jr (1997). *Science*, **277**, 202–206.

Murshudov, G. N., Skubák, P., Lebedev, A. A., Pannu, N. S., Steiner, R. A., Nicholls, R. A., Winn, M. D., Long, F. & Vagin, A. A. (2011). *Acta Cryst.* D**67**, 355–367.

Ochiai, T., Fukunaga, N. & Sasaki, S. (1979). *J. Biochem.* **86**, 377–384.

Ohman, R. & Ridell, M. (1996). *Tuber. Lung Dis.* **77**, 454–461.

Oppenheimer, N. J. (1987). *Pyridine Nucleotide Coenzymes*, Part *A*, edited by D. Dolphin, O. Avramovic & R. Poulson, pp. 323–365. New York: Wiley.

Painter, J. & Merritt, E. A. (2006). *J. Appl. Cryst.* **39**, 109–111.

Peng, Y., Zhong, C., Huang, W. & Ding, J. (2008). *Protein Sci.* **17**, 1542–1554.

Ragland, T. E., Kawasaki, T. & Lowenstein, J. M. (1966). *J. Bacteriol.* **91**, 236–244.

Ramakrishnan, C. & Ramachandran, G. N. (1965). *Biophys. J.* **5**, 909–933.

Reinscheid, D. J., Eikmanns, B. J. & Sahm, H. (1994). *J. Bacteriol.* **176**, 3474–3483.

Rossmann, M. G., Moras, D. & Olsen, K. W. (1974). *Nature (London)*, **250**, 194–199.

Schomaker, V. & Trueblood, K. N. (1968). *Acta Cryst.* B**24**, 63–76.

Shiio, I. & Ozaki, H. (1968). *J. Biochem.* **64**, 45–53.

Singh, S. K., Matsuno, K., LaPorte, D. C. & Banaszak, L. J. (2001). *J. Biol. Chem.* **276**, 26154–26163.

Steen, I. H., Madsen, M. S., Birkeland, N. & Lien, T. (1998). *FEMS Microbiol. Lett.* **160**, 75–79.

Stoddard, B. L., Cohen, B. E., Brubaker, M., Mesecar, A. D. & Koshland, D. E. Jr (1998). *Nature Struct. Biol.* **5**, 891–897.

Stoddard, B. L., Dean, A. & Koshland, D. E. Jr (1993). *Biochemistry*, **32**, 9310–9316.

Stoddard, B. L. & Koshland, D. E. Jr (1993). *Biochemistry*, **32**, 9317–9322.

Sundaralingam, M. (1969). *Biopolymers*, **7**, 821–860.

Taylor, A. B., Hu, G., Hart, P. J. & McAlister-Henn, L. (2008). *J. Biol. Chem.* **283**, 10872–10880.
Vriend, G. (1990). *J. Mol. Graph.* **8**, 52–56.
Wang, Z., Brämer, C. & Steinbüchel, A. (2003). *FEMS Microbiol. Lett.* **227**, 9–16.
Wicken, J. S., Chung, A. E. & Franzen, J. S. (1972). *Biochemistry*, **11**, 4766–4778.
Wierenga, R. K., De Maeyer, M. C. H. & Hol, W. G. J. (1985). *Biochemistry*, **24**, 1346–1357.
Winn, M. D. *et al.* (2011). *Acta Cryst.* D**67**, 235–242.
Winn, M. D., Isupov, M. N. & Murshudov, G. N. (2001). *Acta Cryst.* D**57**, 122–133.
Xu, X., Zhao, J., Xu, Z., Peng, B., Huang, Q., Arnold, E. & Ding, J. (2004). *J. Biol. Chem.* **279**, 33946–33957.
Yang, B., Zhong, C., Peng, Y., Lai, Z. & Ding, J. (2010). *Cell Res.* **20**, 1188–1200.
Yasutake, Y., Watanabe, S., Yao, M., Takada, Y., Fukunaga, N. & Tanaka, I. (2002). *Structure*, **10**, 1637–1648.
Yasutake, Y., Watanabe, S., Yao, M., Takada, Y., Fukunaga, N. & Tanaka, I. (2003). *J. Biol. Chem.* **278**, 36897–36904.
Zhang, B., Wang, B., Wang, P., Cao, Z., Huang, E., Hao, J., Dean, A. M. & Zhu, G. (2009). *Biochimie*, **91**, 1405–1410.
Zheng, J. & Jia, Z. (2010). *Nature (London)*, **465**, 961–965.